minerals

MDPI

Article

Effect of Mg(II) and Na(I) Doping on the Electronic Structure and Mechanical Properties of Kaolinite

Jian Zhao [1], Xinzhan Qin [1,2,*], Jiamin Wang [1] and Manchao He [1]

[1] State Key Laboratory of Geomechanics and Deep Underground Engineering, China University of Mining and Technology, Beijing 100083, China; zhaojiancumtb@163.com (J.Z.); jasmin1029@163.com (J.W.); manchaohecumtb@163.com (M.H.)

[2] School of Civil, Environmental and Mining Engineering, The University of Adelaide, Adelaide 5005, Australia

* Correspondence: bqt1800605056@student.cumtb.edu.cn; Tel.: +86-1521-056-7994

Received: 5 March 2020; Accepted: 15 April 2020; Published: 20 April 2020

Abstract: Because kaolinite has multiple defects, it is very important to study the effect of different doped cations on the electronic structure and mechanical properties of kaolinite ($Al_4Si_4O_{18}H_8$) from the microscopic point of view with the first-principle calculation method. The results exhibited that the doping of Mg(II) and Na(I) makes the ion bond and layer spacing of kaolinite crystal change, and the bond length of the chemical bond between the doped and O atom is positively related to the atomic radius of the doped cations. Compared with undoped kaolinite crystal, the band gap width of the Mg-doped and Na-doped kaolinite crystal was larger, but the typical insulator characteristics were still maintained. Compared with undoped kaolinite crystal, Mg-doped and Na-doped kaolinite crystal had more electron transfer to O, while the Mg–O bond and Na–O bond had more ionic bond properties and less covalent bond composition than the Al–O bond. Finally, the elastic properties of undoped, Mg-doped, and Na-doped kaolinite crystal were further analyzed by calculating the elastic constant matrix. The influence of doping Mg(II) and Na(I) on C_{11} and C_{22} was greater than that on C_{33}, indicating that doping had a greater influence on the stiffness in the direction of the parallel crystal plane. The doping of Mg(II) and Na(I) weakened the rigidity of kaolinite crystal materials and improved the plasticity and ductility of the materials. The atom-scale information provided a basis for explaining the mechanical behavior of kaolinite and is expected to provide guidance for solving the deformation problems in soft rock roadways.

Keywords: kaolinite; clay minerals; electronic structure; mechanical properties; first-principles calculations

1. Introduction

As one of the most important clay minerals in soft rock tunnels [1–3], it is very important to analyze the structural characteristics and mechanical properties of kaolinite for related issues in the field of mineral exploitation and development [4]. However, it is very difficult to determine the atomic structure and mechanical properties of the kaolinite by the experimental method because of its very fine particle size and the complexity of its compositional structure. The theoretical analysis of the electronic mechanical properties of clay minerals from the micro-perspective will help to solve the engineering problems. The first-principle calculation method has been proved to be a very powerful tool for studying the mechanical and electronic properties of kaolinite at the molecular level [5–7].

In fact, there are a large number of defects and impurities in kaolinite crystals in nature. Impurity substitution is a common and important form of impurity entry. After the external impurity atoms and ions enter into the interior of kaolinite, due to the difference of the electric charge between the impurity elements and the substituted elements, redundant electrons and holes appear in the crystal. Thus, the physico-chemical properties of kaolinite crystal are affected to a certain extent. Therefore, it is

very important to investigate the effect of substitutive impurities on kaolinite. At present, there has been some experimental and theoretical research on the effect of substituting impurities on kaolinite at home and abroad [8–11], such as $Fe_{Al\,(Si)}$ (which shows that the Al and Si atoms in kaolinite crystal are replaced by foreign Fe atoms, as well as the role of $Mg_{Al\,(Si)}$ in nature and artificial kaolinite. In 2009, He, M.C. et al. [12] studied the formation energies and transition energy level of the various defects in kaolinite by using the first-principles method. Afterwards, He, M.C. et al. [13–15] analyzed the electronic structure characteristics of kaolinite, such as the energy band structure and density of state, and calculated the transition energy levels and impurity formation energy of the dual defects in kaolinite.

As proven by previous experiments, the introduction of substituted cations into kaolinite change the atomic and electronic structure, and mechanical properties of kaolinite due to the difference of the mass and size between the object atom and the host atom. However, it is not clear which element has a greater influence on the electronic structure and mechanical properties. Therefore, it is of great significance to study systematically the effects of different doped cations with different ion radiuses and atomic masses on the electronic structure and mechanical properties of the material from a micro-perspective. The effect of doped cations on the atomic and electronic structure and mechanical properties of kaolinite were systematically investigated by using the first-principles calculations, which provided theoretical support for solving the problem of large deformations in deep mines in practical engineering.

In order to understand the influence of the cation radius and atomic mass on the mechanical properties of kaolinite, two kinds of metal cations with a higher content were selected to be mixed into kaolinite. As the Al atom was more easily replaced by some cations than the Si atom, the Al atom was used as the core atom. In this paper, Mg and Na were selected to replace Al in kaolinite crystals. The substituted cations could serve as a trapping site for electrons or holes, thereby providing an adsorption center for water molecules. According to a previous calculation [12], Mg_{Al} and Na_{Al} have lower transition energy levels in the process of structural optimization. So, the Mg(II) and Na(I) were ideal donor elements. Therefore, it was of great significance to investigate the influence of Mg(II) and Na(I) replacement in kaolinite crystal. The structural parameters, atomic and electronic structures, and mechanical properties of undoped, Mg-doped, and Na-doped kaolinite crystal were studied by the density functional theory (DFT) method. The atomic origin of the changes of mechanical properties and electronic structures caused by doping ions was explored in this paper.

2. Materials and Methods

In the calculation of substitution impurities of kaolinite, we used the supercell and considered the periodic arrangement of crystal structure. All the calculations were carried out in a $2 \times 1 \times 1$ supercell. The periodic density functional theory calculations were performed using the local density approximation (LDA) in the Vienna Ab-initio Simulation Package (VASP) [16]. The Kohn–Sham equations were solved by using the projector-augmented wave pseudopotentials. The positions of all the atoms were relaxed according to the Hartree fork force. The cutoff energy of the plane wave function was set to 400 electron volt (eV) and the *k*-point grid of the Brillouin region was set to $7 \times 5 \times 5$. The valence electrons of kaolinite included 1 s^1 of H, 2 s^2 2 p^4 of O, 3 s^2 3 p^1 of Al, and 3 s^2 3 p^2 of Si. The valence electrons of alkali metal atoms to be considered in the kaolinite model included 2 p^6 3 s^2 of Mg and 2 p^6 3 s^1 of Na due to heterovalent substitution. The geometry of the atom was optimized by the conjugate gradient algorithm until the Hellman–Feyman force was less than 0.01 eV $Å^{-1}$ to obtain the optimized and stable structure of kaolinite. Many scholars have studied the effect of heterovalent substitution on the mechanical properties of material crystals [17–19]. In 2019, Gao, X.Y. et al. [20] investigated the influence of La, Ge, Pr, and Nd doping on electronic structure and elastic properties of diopside. In the same year, Islam, M.N. et al. [21] studied the influence of Ni doping in a lead halide and a lead-free halide perovskites for optoelectronic applications, and the result showed that undoped and Ni-doped lead and lead-free halides were found to have a direct band gap, mechanical

stability, and ductility. Zhang, Y.M. et al. [22] investigated the structure evolution, elastic, and electronic properties of Pt-doped Ti alloy under pressure.

Based on the stable configuration of kaolinite, different octahedral displacement models were obtained, and the crystal structure characteristics such as the bond length between atoms and layer spacing were calculated. Due to the close relationship between the structure and properties of the material and its microelectronic structure, i.e., the position distribution and energy distribution of electronic states in order to analyze the electronic structure information of different kaolinite crystals intuitively, the band structure, density of electronic state, and charge density of different models were calculated, respectively. The elastic property was the inherent property of the material itself, which represented the deformation extent of the material under the applied stress [23,24]. In order to better understand the influence of doping elements on kaolinite, we systematically studied the mechanical properties of different kaolinite forms, including the bulk modulus, shear modulus, Young's modulus, Poisson's ratio, and other elastic constants, as well as anisotropy and wave velocity.

3. Results

3.1. Effect on Crystal Structure of Kaolinite

The microscopic mechanisms of the Mg(II) and Na(I) doping in kaolinite were studied first before considering the influence of doping on the elastic properties. The atomic structure for the relaxed kaolinite was calculated and numbered (Figure 1), during which the high-symmetry doping site for Mg(II) and Na(I) to substitute for the Al_2 atom in kaolinite was considered.

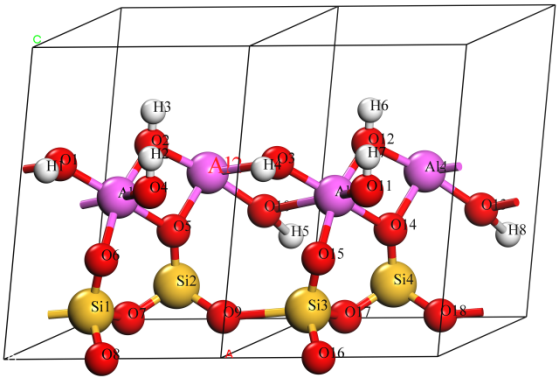

Figure 1. Unit cell of kaolinite ($Al_4Si_4O_{18}H_8$) containing 34 atoms.

According to the previous experimental data [25–27] and calculated results [28,29], the kaolinite consisted of dioctahedral 1:1 layer structures with an ideal composition of $Al_4Si_4O_{10}(OH)_8$ [30,31]. The unit crystal layer was composed of a silicon oxygen tetrahedron (SiO_4) and an aluminum oxygen octahedron ($AlO_4(OH)_2$) [32,33]. All the top oxygen atoms of the silicon oxygen tetrahedron layer pointed in the same direction and were connected with the Al in the aluminum oxygen octahedron. Only two-thirds of the center positions of the aluminum oxygen octahedron were occupied by the Al, and the remaining one-third formed the vacancy; the occupied octahedron and the vacancy were regularly intersected. This could be arranged for other instances. Four of the six oxygen atoms linked to Al were hydroxyl oxygen (O_H), and the remaining two were top oxygen (O_a). According to the position of the hydroxyl, it could be divided into interlayer hydroxyl and internal hydroxyl. The three oxygen atoms of the silicon ring system were called bottom oxygen (O_b). The crystal cell of kaolinite used to calculate the electronic structure included 34 atoms, namely four Al atoms, four Si atoms, eight H atoms, and 18 O atoms. Table 1 lists the optimal structural parameters of the kaolinite model. The calculated structural parameters were a = 5.155 Å, b = 5.155 Å, c = 7.405 Å, α = 75.14°, β = 84.12°, and γ = 60.18°, as shown in Table 1. The DFT calculation results of kaolinite crystal were in good

agreement with the experimental data [19], indicating that the DFT method adopted in this paper was reliable, laying a foundation for the subsequent reliable doping results.

Table 1. Calculated vs. experimental lattice parameters of kaolinite ($Al_4Si_4O_{18}H_8$) using basis sets described in the present study.

Phase	*a*	*b*	*c*	*α*	*β*	*γ*	*V*
Calculated	5.149 Å	8.934 Å	7.384 Å	91.930°	105.042°	89.698°	327.840 Å^3
Exp. [25]	5.155 Å	8.945 Å	7.405 Å	91.700°	104.862°	89.822°	328.710 Å^3
Difference	0.126%	0.122%	0.281%	0.251%	0.172%	0.138%	0.265%

The average calculated bond length of the kaolinite model is listed in Table 2, and the calculated value of DTF matched well with the experimental value [34]. The Al–O bond length in kaolinite was longer than the Si–O bond length, which means that the strength of the Al–O bond was weaker than the Si–O bond, which can partly explain why the Al ion in an octahedral position in kaolinite was more easily replaced by some cations than in a tetrahedral position. The Si–O_a connected to the alumina octahedron was shorter than the Si–O_b bond not connected to the alumina octahedron; similarly, the Al–O_a connected to the silica tetrahedron was shorter than the Al–O_b not connected to the silica tetrahedron. The calculation results exhibited that the ionic bond of kaolinite along the *c* axis was weaker than that along the *a*,*b* plane. The results can partly explain why the large deformation of lattice in kaolinite is always observed along the *c* axis.

Table 2. Calculated vs. experimental average bond length of the undoped kaolinite ($Al_4Si_4O_{18}H_8$), Mg-doped kaolinite ($Al_3MgSi_4O_{18}H_8$), and Na-doped kaolinite ($Al_3NaSi_4O_{18}H_8$).

Phase	O_H–H	Al_2–O_H	Mg–O_H	Na–O_H	Al_2–O_a	Mg–O_a	Na–O_a	Si_2–O_a	Si_2–O_b
Exp. [34]	0.750	1.921	-	-	1.971	-	-	1.610	1.620
$Al_4Si_4O_{18}H_8$	0.970	1.874	-	-	1.995	-	-	1.615	1.637
$Al_3MgSi_4O_{18}H_8$	0.970	-	2.017	-	-	2.095	-	1.601	1.556
$Al_3NaSi_4O_{18}H_8$	0.980	-	-	2.243	-	-	2.255	1.599	1.550

Table 2 also shows the average calculated bond length of the Mg-doped and Na-doped kaolinite crystal. The doping cations had the greatest effect on the Al_2–O bond length, but had little effect on the Si–O and O–H bond. Further, we compared the influence of Mg(II) and Na(I) on the average bond length, which was in the following order: Na–O_H > Mg–O_H > Al_2–O_H, Na–O_a > Mg–O_a > Al_2–O_a, and the change trend of the Si–O bond was opposite. Because Na had the largest ion radius, the bond length of the Na–O bond was also the largest. At the same time, the larger ion radius of Na "pushed" the top oxygen (O_a) outward, making the top oxygen (O_a) closer to the tetrahedral Si, so the Si–O bond had a small degree. From this, we could see that the average bond length of the doped atom and the O atom was positively related to the atomic radius of the doped atom.

From the change of average bond length, it could be seen that the type of replacement cation was an important factor affecting bond length. Therefore, it was necessary to study the change rate of the atomic layer spacing of the Mg-doped and Na-doped kaolinite crystal relative to that of the undoped kaolinite crystal. This is listed in Table 3, where Δd_{ij} represents the atomic layer spacing of layer *i* and layer *j*. From the table, we can see that the doping cations had a great influence on the related Δd_{23} and Δd_{34}, but had a little influence on the distant Δd_{12}, Δd_{45}, and Δd_{56}. The influence of Na(I) on the atomic layer spacing was greater than that of Mg(II); that is, the change of the atomic layer spacing was also related to the atomic radius of the doped atom.

Table 3. Relative to the undoped kaolinite ($Al_4Si_4O_{18}H_8$), the statistics of atomic layer change rate of Mg-doped kaolinite ($Al_3MgSi_4O_{18}H_8$) and Na-doped kaolinite ($Al_3NaSi_4O_{18}H_8$).

Doped Kaolinite	Δd_{12}(%)	Δd_{23}(%)	Δd_{34}(%)	Δd_{45}(%)	Δd_{56}(%)
$Al_3MgSi_4O_{18}H_8$	−0.62	7.01	2.14	−1.48	−0.09
$Al_3NaSi_4O_{18}H_8$	−0.15	11.27	5.31	−3.36	−1.74

3.2. Effect on the Electronic Structure of Kaolinite

To better understand the influence of substitutional impurities on the interaction of various elements in kaolinite crystals, the band structure, density of states, and charge density of different doped kaolinite crystals were analyzed.

The band theory of solids simplifies the motion of electrons in crystals into independent motion in an equivalent potential field, i.e., single electron approximation. The separate energy levels of each atom in the crystal became very dense and split into a series of quasi-continuous energy bands. Each band consisted of N atoms. Each energy level could be occupied with two electrons of opposite spin according to the Pauli exclusion principle, so each band could hold up to 2N electrons. At absolute zero, the electrons in an insulator crystal would fill the energy levels in turn from low to high. In the band structure, one band was completely filled with electrons, had the highest energy, and was termed the valence band, and the next higher energy band was termed the conduction band. The energy separation between the highest valence band state (valence band maximum) and the lowest conduction band state (conduction band minimum) was called the band gap, and their energy difference was termed the band gap width.

The band gap width determined the conductivity of the material. The band gap width of the metal conductor was very small or zero; however, the band gap width of the insulator was large (about 3–6 eV). The band gap width of the semiconductor was between the conductor and the insulator, at about 0.1–2 eV. The energy band structure diagrams of the undoped, Mg-doped, and Na-doped kaolinite crystal are shown in Figure 2. In the energy band structure diagram, the transverse axis is the high symmetry point in the simple Brillouin region, which is Γ(0,0,0), B(0.5,0,0), F(0,0.5,0), and G(0,0,0.5), and the vertical axis is the energy. The above results exhibited that the energy band structure of the kaolinite was relatively flat and its Fermi energy level was located at the valence band maximum (VBM). The VBM values of the undoped, Mg-doped, and Na-doped kaolinite were at the G(0,0,0.5) in the Brillouin zone, and the conduction band minimum (CBM) values were at the Γ(0,0,0) in the Brillouin zone. The indirect band gap width of the undoped kaolinite was 4.99 eV, that of the Mg-doped kaolinite was 5.03 eV, and that of the Na-doped kaolinite was 5.12 eV. Therefore, kaolinite doped with different elements had typical insulator characteristics. The order of the band gap width of each crystal was $Al_4Si_4O_{18}H_8$ < $Al_3MgSi_4O_{18}H_8$ < $Al_3NaSi_4O_{18}H_8$. That is, the doping of Mg(II) and Na(I) made it more difficult for electrons to obtain enough energy to move from the valence to conduction band state.

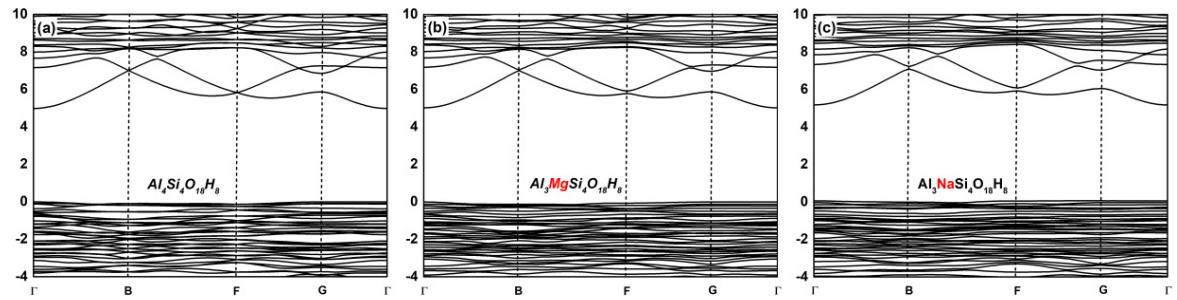

Figure 2. The band structure of the undoped kaolinite and doped kaolinite along high-symmetry lines in the Brillouin zone. (**a**) The band structure of the undoped kaolinite ($Al_4Si_4O_{18}H_8$), (**b**) the band structure of Mg-doped kaolinite ($Al_3MgSi_4O_{18}H_8$), and (**c**) the band structure of Na-doped kaolinite ($Al_3NaSi_4O_{18}H_8$).

In solid-state physics, the density of state, as a visualization result of band structure, can reflect the distribution of electrons in each orbit, as well as the interaction between atoms, and reveal the information of chemical bonds. In Figure 3, we plot the total and partial density of states of the undoped, Mg-doped, and Na-doped kaolinite crystal to understand the effect of Mg(II) and Na(I) doping on the bonding and electronic structure of kaolinite. We set the Fermi energy E_F to 0 eV. Due to the different symmetry and positions, the partial density of state values of different types of oxygen atoms are plotted in Figure 3. The partial density of state values of different oxygen atoms had similar change trends, which may be due to the high ionic degree of oxygen atoms. As shown in Figure 3, the valence band of 10 eV < E < E_F was mainly composed of the O 2*p* state, which implied a large amount of charge transfer from Al 3*p*, Si 3*p* and H 1*s* states to O 2*p* states. The 2*s* and 2*p* states of O bonded with Mg and O adjacent to Al had higher peaks, indicating that Mg is more metallic than Al and had more electron transfer to O. In the same way, the 2*s* and 2*p* states of the Na-bound O and the O adjacent to Mg had higher peaks, indicating that Na was more metallic than Mg and had more electrons transferred to the O adjacent to it.

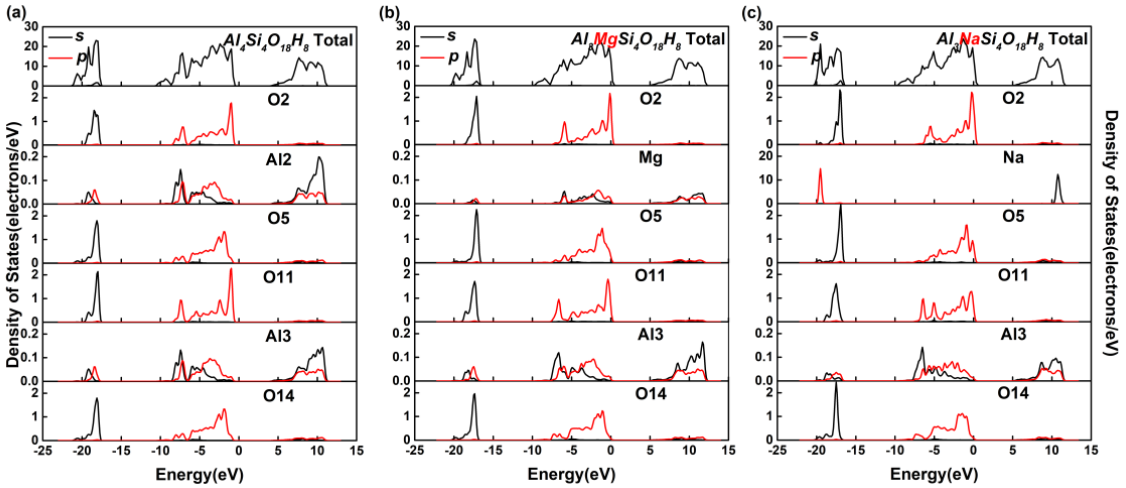

Figure 3. The total and partial density of states of the undoped, Mg-doped, and Na-doped kaolinite. (**a**) The undoped kaolinite ($Al_4Si_4O_{18}H_8$), (**b**) the Mg-doped kaolinite ($Al_3MgSi_4O_{18}H_8$), (**c**) the Na-doped kaolinite ($Al_3NaSi_4O_{18}H_8$).

On the other hand, it can be seen from Figure 3 that some residual charges existed in the 3*s*/3*p* states of Al and Si atom of kaolinite crystal, which means that there were obvious covalent components in the chemical bonds of Al–O and Si–O in kaolinite. At the same time, under the action of a local electric field, the overlap degree of the 3*p* orbit of Mg and 2*p* orbit of adjacent O was lower than that of Al, which made the covalent bond composition of Mg–O lower than that of Al–O. There was almost no overlap between the 3*p* orbit of Na and 2*p* orbit of the adjacent O, and the covalent bond composition of Na–O was very small. In other words, the doping of Na(I) and Mg(II) reduced the covalent bond composition of the crystal.

To better understand the bonding characteristics between atoms in the kaolinite system, a charge density analysis of kaolinite crystal was carried out. Figure 4a shows the charge density diagram of the plane of O_2–Al_2–O_5 in the undoped kaolinite crystal. Figure 4b,c shows the charge density diagram of the plane of O_2–Mg–O_5 in the Mg-doped kaolinite and that of O_2–Na–O_5 in the Na-doped kaolinite, to aid in understanding the influence of doping atoms on the bonding and electronic structure of kaolinite more intuitively and vividly. It can be seen from the Figure 4 that the charge density of Na is smaller than that of Mg and Al. The localization of the charge density of O is stronger, and the charge density around O is more and more disorientated towards the direction of the doped atom (Mg/Na). This shows that the covalent bond properties of the Mg–O bond and Na–O bond are weaker than that of the Al–O bond, and the ionic bond properties are stronger.

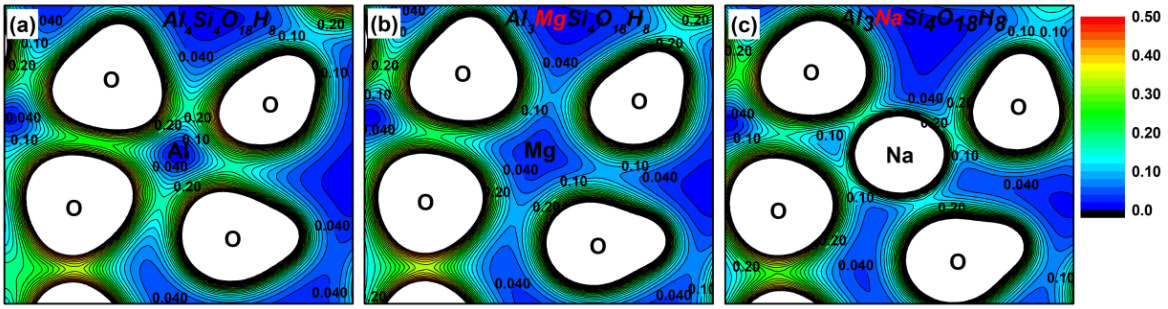

Figure 4. The charge density distribution of the undoped kaolinite and doped kaolinite. The spacing between each contour line is 0.02 eV. (**a**) The O_2–Al_2–O_5 plane in the undoped kaolinite ($Al_4Si_4O_{18}H_8$), (**b**) the O_2–Mg–O_5 plane in the Mg-doped kaolinite ($Al_3MgSi_4O_{18}H_8$), (**c**) the O_2–Na–O_5 plane in the Na-doped kaolinite ($Al_3NaSi_4O_{18}H_8$).

3.3. Effect on the Mechanical Properties of Kaolinite

The elastic constant matrix of the undoped kaolinite was obtained by density functional theory and the VASP software package. So as to evaluate the effectiveness and rationality of the calculation method and parameter setting, the elastic matrix constant of the undoped kaolinite was calculated first and compared with the existing experimental data [35,36] (see Table 4). The DFT calculation results of the elastic matrix constant of kaolinite crystal were in good agreement with the experimental data. According to the calculation results in Table 4, the elastic constants of the undoped kaolinite crystals met the mechanical stability conditions. The C_{33} of the undoped kaolinite crystal was obviously smaller than C_{11} and C_{22}; that is, the elastic constant related to the elastic property in the direction of vertical crystal surface was obviously smaller than that in the direction of the parallel crystal surface, showing that the van der Waals force effect between crystal layers of the undoped kaolinite crystal was far smaller than the bond effect in the crystal layer.

Table 4. The calculated elastic constants of the undoped kaolinite ($Al_4Si_4O_{18}H_8$), Mg-doped kaolinite, ($Al_3MgSi_4O_{18}H_8$) and Na-doped kaolinite ($Al_3NaSi_4O_{18}H_8$) compared with experimental data.

Elastic Constants	$Al_4Si_4O_{18}H_8$			$Al_3MgSi_4O_{18}H_8$ Calculated (GPa)	$Al_3NaSi_4O_{18}H_8$ Calculated (GPa)
	Exp. [35] (GPa)	Exp. [36] (GPa)	Calculated (GPa)		
C_{11}	126.4	171.51	139.18	128.09	114.48
C_{22}	-	-	170.20	153.08	102.55
C_{33}	57.8	52.62	45.50	44.47	38.39
C_{44}	31.6	14.76	9.66	6.84	3.55
C_{55}	-	-	18.62	16.95	12.48
C_{66}	53.6	66.31	53.60	45.93	20.03
C_{12}	-	-	52.46	49.87	48.98
C_{13}	8.5	27.11	28.30	16.70	13.47
C_{14}	-	-	−4.50	2.33	−2.94
C_{15}	-	-	−35.78	−22.17	−21.40
C_{16}	-	-	−4.50	0.53	−9.76
C_{23}	-	-	11.72	6.73	5.83
C_{24}	-	-	−7.30	−12.86	6.89
C_{25}	-	-	−14.50	−13.35	−13.79
C_{26}	-	-	−25.55	−4.50	5.45
C_{34}	-	-	−3.72	0.85	−4.37
C_{35}	-	-	−4.46	6.60	−9.37
C_{36}	-	-	3.86	0.65	−6.53
C_{45}	-	-	−1.25	1.35	0.75
C_{46}	-	-	−13.18	−11.34	0.89
C_{56}	-	-	2.75	2.03	6.86

The elastic constant matrix of the Mg-doped and Na-doped kaolinite is also listed in Table 4. Comparing the elastic constants of different models, it was obvious that the change of C_{11} and C_{22} in

the Mg-doped and Na-doped kaolinite was greater than that of C_{33}; that is, the influence of doping on the stiffness of parallel crystal plane was greater.

The elastic modulus reflected the ability of the material to resist deformation on the macro scale and reflected the bonding strength between atoms, ions, or molecules on the micro scale. The greater the modulus of elasticity, the greater was the stress required for the material to resist elastic deformation, that is, the greater the stiffness of the material. The bulk modulus (B) is a relatively stable constant, indicating the ability of the material to resist to volume changes. The shear modulus (G) indicates the ability of material to resist shear strain. The greater the shear modulus was, the stronger the material's rigidity was. Young's modulus (E) is the elastic modulus along the longitudinal direction, which is a physical quantity describing the deformation resistance of solid materials. It can be seen from Table 5 that the elastic modulus of the undoped kaolinite crystal calculated by the VASP software package matched the experimental value [37], which provided a guarantee for calculating the mechanical and electronic properties of the Mg-doped and Na-doped kaolinite. By calculation, the bulk modulus (B) of kaolinite crystal was 44.001 GPa, and the bulk modulus (B) of the Mg-doped and Na-doped kaolinite were smaller than that of the undoped kaolinite crystal, which proved that the incompressibility of the octahedral replacement model was weaker. The Young's modulus (E) of the undoped kaolinite crystal was 57.783 GPa, and the values of the Mg-doped and Na-doped kaolinite were smaller than that of the undoped kaolinite crystal, which also proved that the ability of octahedral displacement model materials to resist deformation was reduced. The shear modulus (G) of the kaolinite crystal was 22.552 GPa. Similarly, the shear modulus (G) of the two octahedral displacement models decreased, that is, the rigidity of the material decreased. All the above calculations showed that the doping of Mg(II) and Na(I) reduced the stress required for the material to resist further elastic deformation. The reason for this phenomenon is that the doping of Mg(II) and Na(I) increased the distance between atoms, thus reducing the van der Waals force between the layers and the bonding in the crystal.

Table 5. The calculated bulk modulus (B), shear modulus (G), Young's modulus (E), Poisson's ratio (μ), Vickers hardness (H_v), Pugh's modulus ratio (G/B), Cauchy pressure P_c (C_{12}–C_{44}), compression wave velocity (v_p), and shear wave velocity (v_s) of the undoped kaolinite ($Al_4Si_4O_{18}H_8$), Mg-doped kaolinite ($Al_3MgSi_4O_{18}H_8$), and Na-doped kaolinite ($Al_3NaSi_4O_{18}H_8$), compared with experimental data.

Phase	$Al_4Si_4O_{18}H_8$		$Al_3MgSi_4O_{18}H_8$ Calculated	$Al_3NaSi_4O_{18}H_8$ Calculated
	Exp. [37]	Calculated		
Bulk modulus B (GPa)	47.90	44.001	43.288	30.438
Young's modulus E (GPa)	51.97	57.783	48.791	33.91
Shear modulus G (GPa)	19.70	22.552	18.592	12.900
Poisson's ratio μ	0.319	0.281	0.312	0.315
Vickers hardness H_v (GPa)	-	2.643	1.103	0.264
Pugh's modulus G/B ratio	-	0.513	0.429	0.424
Cauchy pressure P_c (GPa)	-	42.805	43.032	45.432
Compression wave velocity v_p (km/s)	5.51	5.321	5.114	4.284
Shear wave velocity v_s (km/s)	2.84	2.936	2.673	2.229

The brittle toughness of the material was related to the Poisson's ratio (μ), which represented the shear stability of the material. In general, a large Poisson's ratio was more ductile than the resulting material. The calculated value of the Poisson's ratio (μ) of the undoped kaolinite crystal was 0.281, and the Poisson's ratio (μ) of the octahedral displacement models was larger than that of the kaolinite crystal, which proved that the ductility of the Mg-doped and Na-doped kaolinite increased, which means that the plasticity of the material was improved. We often use the Pugh's modulus ratio G/B to predict the brittle ductile behavior of materials. When the ratio of G/B of the material is less than 0.57, it is ductile; otherwise, the material is brittle. The G/B ratio of the kaolinite crystal was 0.513, so the kaolinite material had ductility. The G/B ratio of the octahedral replacement model was significantly smaller than that of the kaolinite crystal, so the doping of Mg(II) and Na(I) made the material show better ductility; that is, the plasticity of the material was greatly improved. The Cauchy pressure P_c

(C_{12}–C_{44}) can also reflect the brittle ductile behavior of the material. The calculated value of P_c of the kaolinite crystal was 42.805 GPa. The values of P_c of the octahedral displacement model were higher than those of the kaolinite crystal, the bonding direction was weaker, the mobility was lower, and the toughness of the material was improved. Finally, the Vickers hardness ($H_{v)}$ could be used to express the hardness of materials. The calculation formula of H_v is $H_v = 2(K^2G)^{0.583} - 3$, where K is the Pugh's modulus ratio G/B. The calculated value of H_v of the kaolinite crystal was 2.643 GPa. The Vickers hardness of the octahedron replacement model decreased, implying that the hardening influence of the material was weakened. The doping of Mg(II) and Na(I) made the elastic wave velocity decrease.

4. Conclusions

The influence of doping Mg(II) and Na(I) cations on the mechanical and electronic structure of kaolinite was calculated in detail by the LDA method based on the first-principle method.

The main conclusions are as follows:

(1) The doping of Mg(II) and Na(I) changed the ionic bond and the atomic layer spacing in kaolinite crystals. The average bond length of the doped atom and the O atom was positively related to the atomic radius of the doped atom. The doping cations had a certain effect on the layer spacing of the Al–O_H layer and Al–O_a layer, but had little effect on the layer spacing of the Si–O_a layer and Si–O_b layer, which were far away from doped atom.

(2) By analyzing the electronic structure of the crystal, the band gap width of the Mg-doped and Na-doped kaolinite increased, which indicated that the doping of Mg(II) and Na(I) made it more difficult for the electrons to obtain enough energy to move from the valence to conduction band state. Compared with Al, Na and Mg had more electron transfer to the adjacent O; that is, the charge density around O decreased in the direction of the doped atom (Mg/Na), the covalent bond composition of Mg–O bond and Na–O bond became weaker than Al–O bond, and the ionic bond properties were stronger.

(3) The influence of doping Mg(II) and Na(I) on C_{11} and C_{22} was greater than that on C_{33}, indicating that doping had a greater influence on the stiffness in the direction of parallel crystal plane. In addition, the doping of Mg(II) and Na(I) reduced the elastic modulus of kaolinite crystal and weakened the rigidity of the material. As the Vickers hardness decreased, the hardening effect of the material weakened. The changes of Poisson's ratio (μ), Pugh's modulus ratio (G/B), and the Cauchy pressure (P_c) indicated that the directivity of atom bonding was weakened, and the plasticity and ductility of the material were improved.

Author Contributions: Conceptualization and methodology, J.Z. and X.Q.; software, J.Z.; validation, formal analysis, data curation and writing, X.Q.; investigation, J.W.; funding acquisition, M.H. All authors have read and agreed to the published version of the manuscript.

Funding: Project supported by the Program for the National Natural Science Foundation of China (No.41702317).

Conflicts of Interest: The authors declare no conflict of interest.

References

1. He, M.C. Latest progress of soft rock mechanics and engineering in China. *J. Rock Mech. Geotech. Eng.* **2014**, *6*, 165–179. [CrossRef]
2. Kanji, M.A. Critical issues in soft rocks. *J. Rock Mech. Geotech. Eng.* **2014**, *6*, 186–195. [CrossRef]
3. Ighil Ameur, L.; Robin, G.; Hattab, M. Elastic properties in a clayey material under mechanical loading-an estimation through ultrasonic propagations. *Eur. J. Environ. Civ. Eng.* **2015**, *20*, 1127–1146. [CrossRef]
4. Bourret, J.; Tessier-Doyen, N.; Guinebretiere, R.; Joussein, E.; Smith, D.S. Anisotropy of thermal conductivity and elastic properties of extruded clay-based materials: Evolution with thermal treatment. *Apply Clay Sci.* **2015**, *116*, 150–157. [CrossRef]
5. LiBalan, E.; Pietrucci, F.; Gervais, C.; Blanchard, M.; Schott, J.; Gaillardet, J. First-principles study of boron speciation in kaolinite and aragonite. *Geochim. Cosmochim. Acta* **2016**, *193*, 119–131.

6. Weck, P.F.; Kim, E.; Jové-Colón, C.F. Relationship between crystal structure and thermo-mechanical properties of kaolinite clay: Beyond standard density functional theory. *Dalton Trans.* **2015**, *44*, 12550–12560. [CrossRef]
7. Fang, Z.J.; Zhai, X.S.; Li, Z.L.; Pan, R.J.; Mo, M. Pressure dependence of the electronic structure in kaolinite: A first-principles study. *Mod. Phys. Lett. B* **2017**, *31*, 1750194. [CrossRef]
8. Prasad, M.; Kopycinska, M.; Rabe, U.; Arnold, W. Measurement of Young's modulus of clay minerals using atomic force acoustic microscopy. *Geophys. Res. Lett.* **2002**, *29*, 13–16. [CrossRef]
9. Vanorio, T.; Prasad, M.; Nur, A. Elastic properties of dry clay mineral aggregate, suspensions and sandstones. *Geophys. J. Int.* **2003**, *155*, 319–326. [CrossRef]
10. He, M.C.; Zhao, J.; Fang, Z.J.; Zhang, P. First-principles study of isomorphic (dual-defect) substitution in kaolinite. *Clays Clay Miner.* **2011**, *59*, 501–506. [CrossRef]
11. Hobbs, J.D.; Cygan, R.T.; Nagy, K.L.; Schultz, P.A.; Sears, M.P. All-atom ab initio energy minimization of the kaolinite crystal structure. *Am. Mineral.* **1997**, *82*, 657–662. [CrossRef]
12. He, M.C.; Fang, Z.J.; Zhang, P. Theoretical studies on defects of kaolinite in clays. *Chin. Phys. Lett.* **2009**, *26*, 059101.
13. He, M.C.; Zhao, J.; Fang, Z.J. First-principles study of atomic and electronic structures of kaolinite in soft rock. *Chin. Phys. B* **2012**, *21*, 039101. [CrossRef]
14. He, M.C.; Zhao, J. Effects of Mg, Ca, and Fe(II) doping on the kaolinite (001) surface with H_2O adsorption. *Clays Clay Miner.* **2012**, *60*, 330–337. [CrossRef]
15. Zhao, J.; He, M.C. Theoretical study of heavy metal Cd, Cu, Hg, and Ni(II) adsorption on the kaolinite(001) surface. *Appl. Surf. Sci.* **2014**, *317*, 718–723. [CrossRef]
16. Kresse, G.; Furthmüller, J. Efficient iterative schemes for ab initio total-energy calculations using a plane-wave basis set. *Phys. Rev. B.* **1996**, *54*, 11169–11173. [CrossRef]
17. Zhao, F.; Chen, B.; Zhang, C.H. Effect of rare earth (Sc, Y, La, Sm and Gd) doping on mechanical and thermodynamic properties of $Al_{12}Mg_{17}$ intermetallic compounds. *Mod. Phys. Lett. B* **2019**, *33*, 1950442. [CrossRef]
18. Zhang, T.; Yin, H.Q.; Zhang, C.; Yang, Z.; Deng, Z.H.; Yang, G.Q.; Zheng, Q.J.; Qu, X.H. First-principle calculations of mechanical properties and electronic structure of WCoB and Cr doped WCoB under high pressure. *Mater. Res. Express* **2019**, *11*, 116320. [CrossRef]
19. Wang, N.; Liu, H.F. First-principles study of electronic structure and optical properties of Ca-Doped SnS_2. *Mater. Sci.* **2018**, *8*, 1094–1101.
20. Gao, X.; Wang, H.; Wang, C.; Chen, S.; Zhao, M.; Li, B. First-principles investigation of the effects of Re (La, Ce, Pr and Nd) doping on the diopside phase of glass–ceramics. *J. Non-Cryst. Solids* **2019**, *526*, 119701. [CrossRef]
21. Islam, M.N.; Hadi, M.A.; Podder, J. Influence of Ni doping in a lead-halide and a lead-free halide perovskites for optoelectronic applications. *AIP Adv.* **2019**, *9*, 125321. [CrossRef]
22. Zhang, Y.; Zhao, Y.; Duan, M.; Hou, H. Structure evolution, elastic and electronic properties of Pt-Doped Ti alloy under pressure. *Phys. Status Solidi (b)* **2019**, *257*, 1900360. [CrossRef]
23. Sachse, W.; Ruoff, A.L. Elastic moduli of precompressed pyrophyllite used in ultrahigh, ressure research. *J. Appl. Phys.* **1975**, *46*, 3725–3730. [CrossRef]
24. Pawley, A.; Clark, S.; Chinnery, N. Equation of state measurements of chlorite, pyrophyllite, and talc. *Am. Mineral.* **2002**, *87*, 1172–1182. [CrossRef]
25. Adams, J.M. Hydrogen atom position kaolinite by neutron profile refinement. *Clays Clay Miner.* **1983**, *31*, 352–358. [CrossRef]
26. Benco, L.; Tunega, D.; Hafner, J.; Lischka, H. Orientation of OH groups in kaolinite and dickite: Ab initio molecular dynamics study. *Am. Mineral.* **2001**, *86*, 1057–1065. [CrossRef]
27. Bish, D.L. Rietveld refinement of the kaolinite structure at 1.5 K. *Clays Clay Miner.* **1993**, *41*, 738–744. [CrossRef]
28. Hess, A.C.; Saunders, V.R. Periodic ab initio hartree-fock calculations of the low-symmetry mineral kaolinite. *J. Phys. Chem.* **1992**, *96*, 4367–4374. [CrossRef]
29. Hu, X.L.; Angelos, M. Water on the hydroxylated (001) surface of kaolinite: From monomer adsorption to a flat 2D wetting layer. *Surf. Sci.* **2008**, *602*, 960–974. [CrossRef]
30. Bailey, S.W. Summary of recommendations of AIPEA nomenclature committee. *Clay Miner.* **1980**, *15*, 85–93. [CrossRef]

31. Schwieger, W.; Bergk, K.H.; Heidemann, D.; Lagaly, G.; Beneke, K. High-resolution Si-29 solid-state NMR-studies on A synthetic sodium-silicate hydrate (makatite) and its crystalline silicic-acid. *Z. Fur Krist.* **1991**, *197*, 1–12. [CrossRef]
32. Giese, R.F., Jr. Interlayer bonding in kaolinite dickite and nacrite. *Clays Clay Miner.* **1973**, *21*, 145–149. [CrossRef]
33. Hajjaji, W.; Andrejkovicova, S.; Pullar, R.C.; Tobaldi, D.M.; Lopez-Galindo, A.; Jammousi, F.; Rocha, F.; Labrincha, J.A. Effective removal of anionic and cationic dyes by kaolinite and TiO_2/kaolinite composites. *Clay Miner.* **2016**, *51*, 19–27. [CrossRef]
34. Neder, R.B.; Burghammer, M.; Grasl, T.H.; Schulz, H.; Bram, A.; Fiedler, S. Refinement of the kaolinite structure from single-crystal synchrotron data. *Clays Clay Miner.* **1999**, *47*, 487–494. [CrossRef]
35. Wenk, H.R.; Voltolini, M.; Mazurek, M.; Van Loon, L.R.; Vinsot, A. Preferred orientations and anisotropy in shales: Callovo-Oxfordian shale (France) and opalinus clay. *Clays Clay Miner.* **2008**, *56*, 285–306. [CrossRef]
36. Katahara, K.W. Clay mineral elastic properties. *SEG Tech. Progr. Expand. Abstr.* **1999**, *15*, 1691–1694.
37. Wang, Z.; Wang, H.; Gates, M.E. Effective elastic properties of solid clays. *Geophysics* **2001**, *66*, 428–440. [CrossRef]